Eng. Sci., 2024, **32**, 1254

Engineered Science
DOI: https://dx.doi.org/10.30919/es1254

Influence of Synthesis Conditions on the Physical Characteristics and Antibacterial activities of Cerium Oxide Nanoparticles in Biomedical Applications

Swapnaja S. Gajbhiye,[1, 2] Maruti V. Salve,[1] Madhavi D. Gaikwad,[3] Akshada R. Rasage,[3] Maya S. Khater,[3] Vijay H. Ghadage[2] and Nandu B. Chaure[1,*]

Abstract

The present work aims to describe the influence of synthesis conditions of cerium oxide nanoparticles (CeO_2 NPs) by a hydrothermal method on physical properties and antibacterial activities. The structural and optical properties of the CeO_2 NPs were investigated using X-ray diffraction (XRD), Raman spectroscopy, and diffuse reflectance spectroscopy. The XRD analysis revealed a cubic crystal structure. The Raman mode at approximately 463 cm^{-1} was identified as the F2g optical phonon mode for the stretching of the Ce-O vibration. Optical energy band gap of the CeO_2 NPs was estimated to be 3.2 to 3.3 eV by UV-Vis diffuse reflectance spectroscopy. The Ce-O stretching behavior was confirmed by Fourier Transform Infrared (FTIR) Spectroscopy. Field emission scanning electron microscopy (FE-SEM) and energy-dispersive X-ray spectroscopy (EDX) were used to examine the morphological features and elemental analysis of the CeO_2 NPs. The antibacterial activity of the CeO_2 NPs was examined using the disc diffusion method. The minimum inhibitory concentration (MIC) values obtained were 500 μg/ml and 1000 μg/ml for 12 h and 24 h treated CeO_2 NPs respectively, against *E. coli*, and 500 μg/ml for 24 h treated CeO_2 NPs against *S. aureus*. No antibacterial activity was observed after 48 h of treatment with CeO_2 NPs.

Keywords: Cerium oxide nanoparticles; Hydrothermal method; Antibacterial activity; Minimum inhibitory concentration.
Received: 01 March 2024; Revised: 31 July 2024; Accepted: 21 August 2024.
Article type: Research article.

1. Introduction

The rise in antibiotic-resistant bacteria necessitates the urgent need for alternative antibacterial agents. Nanoparticles have the potential to revolutionize antibacterial treatment in the medical field. By understanding their antibacterial properties, researchers can design effective therapies to combat bacterial infections that are increasingly resistant to traditional antibiotics.[1] Nanoparticles (NPs) can be used by medical practioners to develop innovative antibacterial treatments. Metal and metal-oxide nanoparticles are promising materials for nanotechnology. The size and shape of the NPs play a significant role in tuning their optical, electrical, and optoelectronic properties. Metal oxide NPs such as bismuth oxide (Bi_2O_3), titanium dioxide (TiO_2), copper oxide (CuO), cerium oxide (CeO_2), and zinc oxide (ZnO) have demonstrated great potential in biomedical applications. In addition, some metal-oxide NPs have emerged as good antibacterial agents. Among these metal oxides, CeO_2 NPs have been employed in sensing,[2] catalysis,[3] supercapacitors,[4] antibacterial,[5] and anticancer[6] applications owing to their physical, chemical, and redox properties. Nevertheless, CeO_2 NPs in such applications are commonly associated with the shape, surface area, and quality of the crystalline structure.

Cerium is a rare earth metal belonging to the lanthanide family and has two oxidation states: Ce^{3+} and Ce^{4+}. The Ce atoms on the surface can either store or release oxygen, engaging in a cyclic transformation between Ce^{3+} and Ce^{+4} ions. CeO_2 (ceria), acknowledged as a notable redox catalyst, functions as a versatile material well suited for diverse applications. Various chemical routes, such asprecipitation,[7] co-precipitation,[8] hydrothermal,[9,10] solvothermal route,[11] laser ablation method,[12] pyrolysis,[13] combustion method,[14] and sol gel method[15] have been reported for the synthesis of

---

[1] Department of Physics, Savitribai Phule Pune University, Pune 411007, India.

[2] Department of Physics, Baburaoji Gholap College, Sangvi, Savitribai Phule Pune University, Pune 411027, India.

[3] Department of Biotechnology, Abasaheb Garware College, Savitribai Phule Pune University, Pune 411004, India.

*Email: nchaure.uop@gmail.com (N. B. Chaure)

CeO_2 NPs. Among these, hydrothermal techniques are promising alternative synthetic methods because of the low process temperature and ease of controlling the particle size and morphology growth. Researchers have obtained various morphological CeO_2 NPs, including nanowires,[16] nanocubes,[17] and nanorods,[18] and investigated their size and shape dependent antibacterial performance. Currently, there is significant interest in utilizing CeO_2 nanoparticles as antimicrobial agents that specifically target bacterial pathogens.[19,20] They combat a variety of bacterial strains, such as *S. aureus*, *E. coli*, and *P. aeruginosa*.[5,10,12,21,22] Nanoparticles can penetrate bacterial cells more effectively than larger particles, making them potentially more efficient at killing bacteria. By adjusting their activity, researchers can optimize their design to maximize their efficacy.[23] The precise mechanism by which microbes are killed has yet to be determined. The biological efficacy of CeO_2 NPs is ascribed to their robust electrostatic characteristics, small size, and unique morphologies.[24,25] Moreover, targeting particular bacterial strains and interfering with their growth pathways is a potential application of nanoparticles. This includes understanding CeO_2 NPs antibacterial mechanisms, efficiency, recent developments, and research challenges, emphasizing the need to stay updated on advancements and their potential in combating bacterial infections.

In this study, we report the successful fabrication of CeO_2 NPs via a hydrothermal route, using cerium nitrate hexahydrate as the cerium source. The structural, optical, and morphological characteristics of the obtained products were analyzed using various characterization techniques. The antibacterial activity of the CeO_2 NPs against *Escherichia coli* and *Staphylococcus aureus* was examined *in vitro* by determining the minimum inhibitory and minimum bactericidal concentrations. However, to the best of our knowledge, synthesized samples have not been used in studies of the Minimum Bactericidal Concentration (MBC) using the drop plate technique and the Minimum Inhibitory Concentration (MIC) using resazurin and also to study the cell morphology of bacteria before and after treatment with CeO_2 NPs.

2. Experimental details

2.1 Materials

For CeO_2 NPs synthesis, cerium nitrate hexahydrate (Ce $(NO_3)_2.6H_2O$; 432.2 g/mole; 99.9% purity, HPLC), sodium hydroxide (NaOH; 40 g/mol; 99.9% purity, Aldrich), double-distilled water (DDW), and ethanol (99% AR grade) were used. For antibacterial activity, Nutrient agar (NA, Hi-Media), sodium chloride (NaCl), and yeast were employed.

2.2 Synthesis of CeO_2 NPs

CeO_2 NPs were synthesized using a cost-effective, one-step hydrothermal method. Fig. 1 shows a schematic representation of the hydrothermal synthesis of CeO_2 Nanoparticles. In a typical synthesis, 1 molar (M) of cerium nitrate hexahydrate was dissolved in DDW. The NaOH solution was gradually introduced dropwise into the cerium nitrate solution to adjust the pH to 8.5. The solution was continuously stirred for 1 hour (h) using a magnetic stirrer. The obtained precipitate was transferred to a Teflon-lined stainless-steel autoclave and maintained at 180 °C for different reaction times (12 h, 24 h, and 48 h). The product was washed several times with DDW and ethanol to remove impurities. The obtained precipitate was dried in a hot air oven for 12 h at 80 °C.

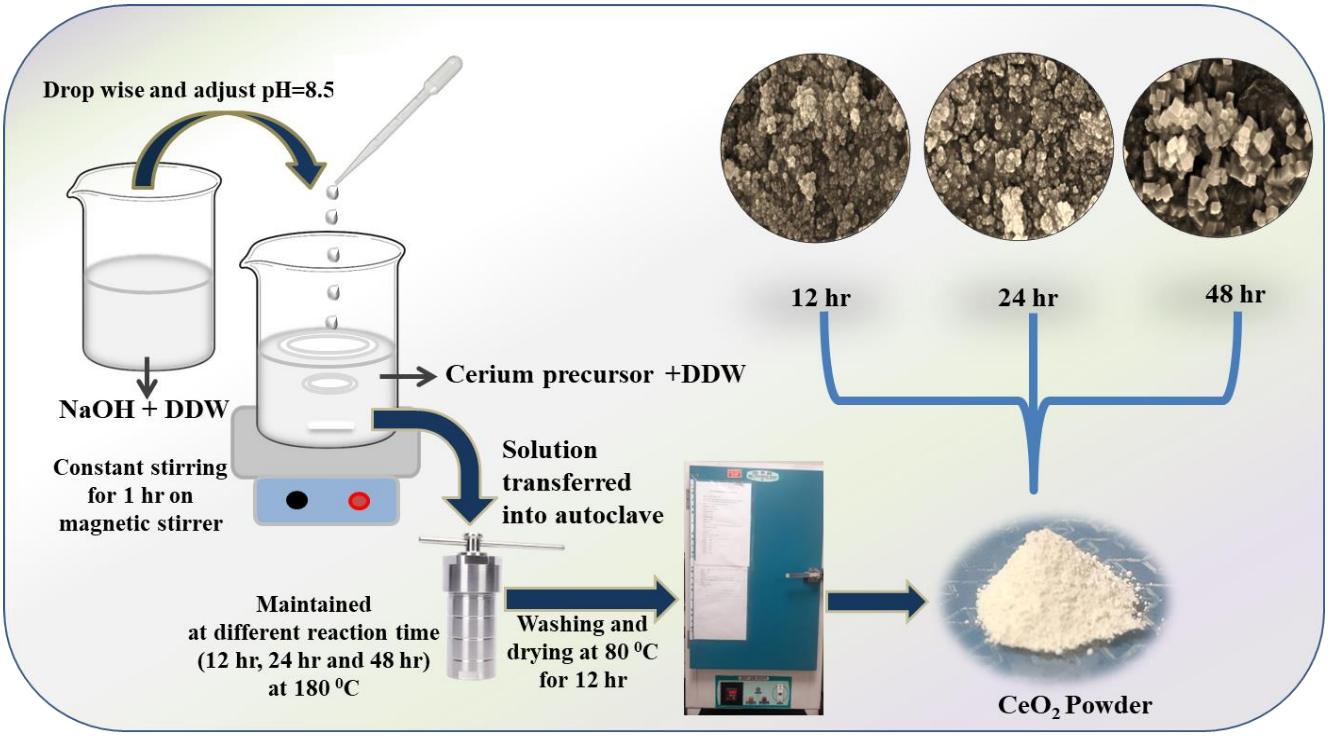

Fig. 1 Schematic representation of the hydrothermal synthesis of CeO_2 nanoparticles.

2.3 Characterization techniques

Structural information was obtained using a Bruker D8 Advanced X-ray diffractometer (XRD) with a Cu Kα anode in the 2θ range of 20°-80°. Raman spectroscopy was performed using InVia Renishaw micro-Raman spectrometer with an excitation wavelength of 532 nm with power 1mW. For optical measurements, a JASCO-770 V UV-Vis-NIR spectrophotometer was used to determine the optical energy bandgap. Fourier transform infrared (FTIR) spectroscopy was performed using an FTIR instrument (SHIMADZU IR-Affinity-1) in the diamond Attenuated Total Reflection (ATR) mode. Field emission scanning electron microscope (FESEM) images were captured using a FEI Nova NANOSEM 450. The surface morphologies of the samples were examined by scanning electron microscopy (SEM) at an operating voltage of 10 kV (JSM 6360-A; JEOL). The elemental compositions of the samples were analyzed using energy-dispersive X-ray analysis (EDX) integrated with an SEM unit.

2.4 Antibacterial activity of CeO_2 NPs

CeO_2 NPs have been investigated for antibacterial activity against Gram-positive bacteria *Staphylococcus aureus* ATCC 6538 and Gram-negative bacteria *Escherichia coli* NCIM 2065. The two bacteria were cultured in nutrient broth (NA) for 24 h at 37 °C until the bacterial suspension reached 1.5×10^8 CFU/ml.[26] In antibacterial studies, the bacterial sample was used as an inoculum.

2.4.1 Disc diffusion method by pour plate technique

The disc diffusion method was used to assess the antibacterial activity of the CeO_2 NPs. A petri dish filled with 20 ml of molten NA was allowed to cool and covered with 0.1 ml of a bacterial solution. Ten different concentrations of CeO_2 NPs, 1000 µg/ml, 500 µg/ml, 250 µg/ml, 125 µg/ml, 62.5 µg/ml, 31.2 µg/ml, 15.6 µg/ml, 7.8 µg/ml, 3.9 µg/ml, 1.9 µg/ml were loaded onto discs through a two-fold dilution and a concentration of 1 mg/ml, using sterile DDW. The discs were then placed on an agar medium using sterile forceps. The negative control consisted of 100 ml of sterile DDW, whereas the positive control consisted of ampicillin. The plates were then incubated at 37 °C for 24 h after measuring the inhibition zone surrounding each disc.

2.4.2 Minimum Inhibitory Concentration (MIC)

The MIC of the CeO_2 NPs was determined using the microtitration method. In general, MIC is defined as the minimum concentration of an antimicrobial agent that prevents the growth of microorganisms under specific conditions.[27] In the analysis, determining MIC, using append off tubes, in which 500 µl of NPs different concentrations, 500 µl of NB and 10 µl of bacterial culture (*Staphylococcus aureus* or *Escherichia coli*) were introduced. The tubes were then incubated for 24 h at 37 °C. After the incubation period, 96 well plates were used, in which 100µL of NPs was used at different concentrations. After the test material was added to each well, tips were discarded. 10 µl of resazurin was then added to each microwell. The plates were then incubated for an additional 3 h. After incubation, the minimum concentration at which the blue color of the resazurin dye remained unaltered was identified as the MIC value for the antibacterial agents. Resazurin serves as an oxidation reduction indicator to assess cell growth.[28,29] The activation of resazurin by bacteria was also indicated by the change in color from blue to pink; therefore, the MIC was determined as the lowest concentration of NPs that inhibited the color change of resazurin.[29,30] In this evaluation, *S. aureus* and *E. coli* untreated control wells, pink color indicates live cells, and ampicillin and purple colors represent dead cells.

2.4.3 Minimum Bactericidal Concentration (MBC)

The MBC was determined after optimizing the MIC. From the tubes, an aliquot of 10 ml sample was seeded on an agar plate using the drop method and incubated at 37 °C for 24 h. The MBC was found to be the lowest concentration following the subculture process at which no visible growth occurred.

2.4.4 Sample Preparation for SEM

Two bacterial strains were used *E.coli* and *S.aureus* in the present study. The bacterial cultures were freshly grown in sterile Nutrient Broth and incubated at 37 °C for 24 h. Samples were prepared by adding 1mg of the nanoparticles sample and 1 ml broth into each appendroff tube, followed by sonication of each samples for 15 -20 min. After sonication, bacterial cultures were suspended in the tubes. Another set was prepared as a control for both bacteria by adding 1ml broth and bacterial suspension into an appendroff tube. Then after, both the sets were kept for 24 h at 37 °C (120 rpm) in shaker incubator. Glass slide was chosen as the substratum in the present study. They were immersed in 99% ethanol solution overnight, then washed by sonication for 10 min in sterilized distilled water, a procedure repeated twice. The washed slides were placed in sterilized petri dishes and dried at room temperature for 12 h. For cell sample fixation, firstly respective samples were smeared on slides. Then after, cells are treated with a solution of 2.5% glutaraldehyde in PBS for 2 h at room temperature. The washing process was followed by serial dehydration using ethanol at 10%, 25%, 40%, 50%, 70%, 90%, and 100% for 5 min each. Subsequent to the dehydration process, it will be air dried for 3-10 h in the biological safety hood without the lid on. All fixation methods were conducted with two duplicates.[31]

3. Results and discussion

3.1. X-ray Diffraction analysis

Figure 2 shows the XRD patterns of ceria powder samples prepared for different durations using the hydrothermal technique. The Bragg reflections are observed at an angle (2θ) of 28.53°, 33.05°, 47.46°, 56.33°, 59.04°, 69.40°, 76.7° and 79.07° corresponds to (111), (200), (220), (311), (222), (400), (331) and (420), planes of CeO_2 of cubic fluorite structure according

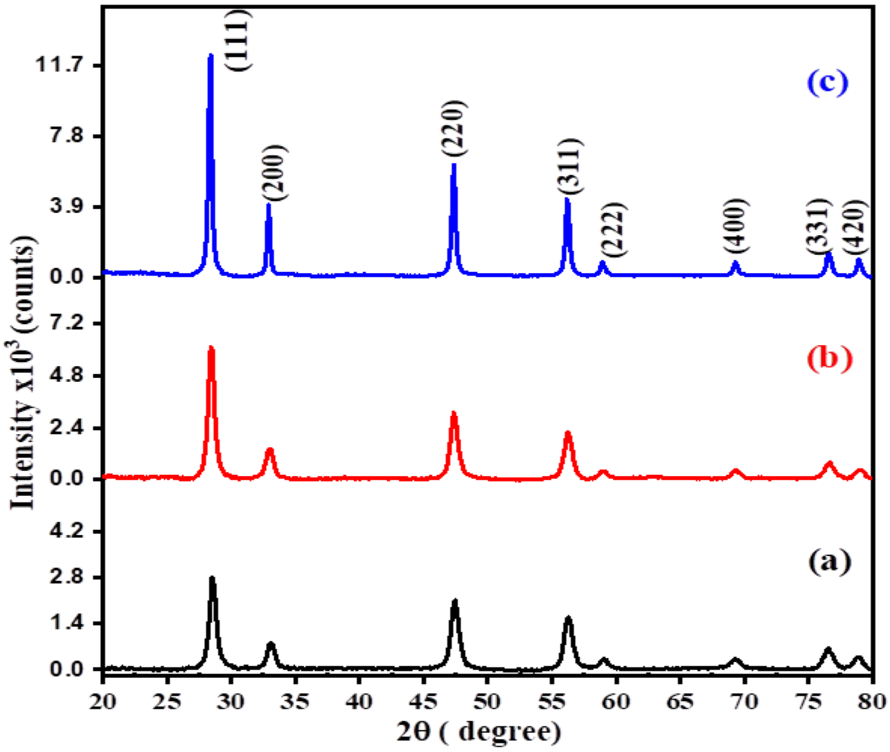

Fig. 2 XRD spectra of CeO_2 NPs for (a) 12 h, (b) 24 h and (c) 48 h.

to JCPDS Card No. 34-0394. Similar results were reported by Pathak *et al.* using a chemical precipitation technique.[32] Li *et al.* employed a hydrothermal technique to synthesize ceria powder samples.[33] In this study, the XRD results indicate more definite patterns with strong, distinct peaks, suggesting that the obtained samples are highly pure and have better structural integrity. No peaks associated with impurities were detected, indicating the purity of the samples. As the reaction time increased, the broadening of the full width at half maximum (FWHM) decreased substantially, illustrating the enhancement in the degree of crystallinity.[34] The improvement in crystallinity has been reported by Tok *et al.* for CeO_2 samples obtained via a hydrothermal technique, owing to the increase in particle size due to the agglomeration of small particles.[35] The structural parameters such as lattice constant, dislocation density, and microstrain of the plane (111) direction were determined using the following Debye Scherrer equation.[36]

$$D = \frac{k\lambda}{\beta\cos\theta} \tag{1}$$

where D is the average crystallite size, k is constant which depends on the shape of the particle (Here we have taken k = 0.9 for spherical shape of the particle), θ is the Bragg angle, λ is the wavelength of incident ray (1.5406 Å), β is the FWHM. The obtained data were used to calculate the interplanar distance (*d*), lattice constant (*a*), dislocation density (δ), and microstrain (ε). The following equations were used for the calculation of above values, and the results are summarized in Table 1.

$$d = \frac{n\lambda}{2\,sin\theta} \tag{2}$$

$$a = d_{hkl}\sqrt{h^2+k^2+l^2} \tag{3}$$

$$Dislocation\ density\ (\delta) = \frac{1}{D^2} \tag{4}$$

$$microstrain\ (\varepsilon) = \frac{\beta\ cos\theta}{4} \tag{5}$$

The average crystallite size increased as the reaction time increased, indicating improved crystallinity of the CeO_2 NPs.[37] The XRD analysis showed that the (111) plane displayed the highest peak intensity, indicating a cubic fluorite structure. Furthermore, the average crystallite size was in the range of 9-19 nm. As presented in Table 1. decreased strain and dislocation density, with microstrain in the lattice, diminished as the particle size increased. This can be ascribed to a reduction in the broadening of the diffraction peaks when the reaction time is extended.[38-40]

3.2. Raman analysis

The Raman spectra depicted in Fig. 3 provide insights into the defects within the structure at various reaction times. It is recognized that bulk ceria displays a sharp peak at 464 cm^{-1}, attributed to the triply degenerate F2g mode, representing a symmetric stretching mode of oxygen atoms surrounding the cerium ions.[41,42] Rajan *et al.* and Pandiyan *et al.* performed the Raman measurement on CeO_2 samples prepared by chemical and biological techniques and observed these peaks at about 461cm^{-1} and 463 cm^{-1} which confirmed cubic fluorite structure for sample (a) and sample (b-c), respectively.[43,44] The peak broadening suggested that the particle size was small. In addition, minor peaks at 191 cm^{-1}, 600 cm^{-1}, 1049 cm^{-1}, 105

Table 1. Structural parameters such as the average crystallite size obtained for preferentially oriented (111) reflections are the d-spacing, lattice constant, dislocation density, and microstrain.

CeO_2 Samples	Average Crystallite size	d-spacing (Å) for (111)	Lattice constant (Å) for (111)	Dislocation density (nm^{-2}) for (111)	microstrain x 10^3 for (111)
12 h (a)	9	3.121	5.4054	0.008197	0.003041
24 h (b)	10	3.134	5.4288	0.006587	0.002643
48 h (c)	19	3.143	5.4442	0.001848	0.001400

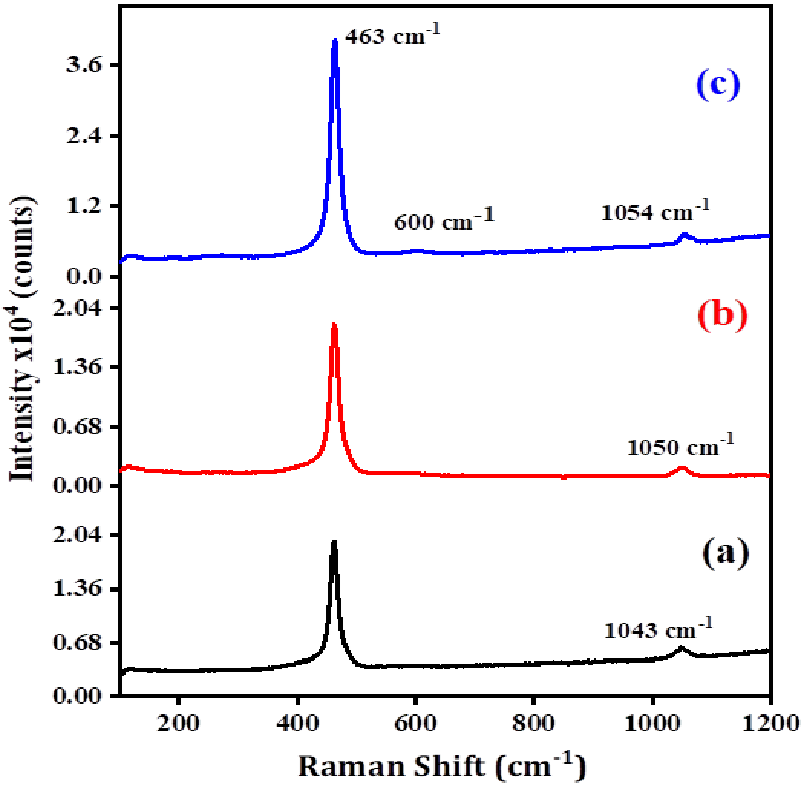

Fig. 3 Raman spectra of CeO_2 NPs after (a) 12 h, (b) 24 h, and (c) 48 h.

-1 cm^{-1}, and 1054 cm^{-1} were observed. Govindarasu *et al.* observed weak bands around 602 cm^{-1} and 1043 cm^{-1}, which may have been associated with the non-degenerate longitudinal optical (LO) phonon mode of CeO_2.[45]

Furthermore, it shows a weak band at approximately 260 cm^{-1} and a shoulder at 600 cm^{-1}, which are typically attributed to Raman inactive (but IR active) transverse and longitudinal optical phonon modes, respectively.[46] In another study, the bands observed at 643 cm^{-1}, 1044 cm^{-1}, 1221 cm^{-1}, and 1377 cm^{-1} were attributed to the presence of oxygen vacancies.[47,48] It was also observed that the peak intensities increased as the FWHM decreased; these results are in agreement with the XRD results.

3.3. UV-Vis-diffused reflectance spectroscopy

Figure 4 depicts the reflectance spectra of CeO_2 NPs. The direct bandgap of the NPs was determined using the Kubelka–Munk (K–M) equation.[49]

$$(F(R)\,h\upsilon)^2 = A(h\upsilon - E_g) \tag{6}$$

where 'h' is a Planck's constant, 'υ' is the light frequency; 'A' is the absorption coefficient and, 'E_g' is the band gap energy.

$$F(R) = \frac{K}{S} = \frac{(1-R)^2}{2R} \tag{7}$$

where F(R) is the ratio of the absorption coefficient (K) to the scattering coefficient (S) and is also known as the K-M function.

As illustrated in Fig. 4, a K-M plot was constructed between $(F(R)h\upsilon)^2$ and hυ, and the bandgap energy values were estimated to be 3.24, 3.27 and 3.26 eV. In our results, bandgap value increases up to 3.27 eV then decrease to 3.26 eV, when reaction time varies. This behavior is most likely due to the formation of oxygen vacancies in the CeO_2 lattice, which allow the formation of localized energy states between the O 2p (valence band) and Ce 4f states. Li et al. found similar results in the literature with bandgap values of 2.73 eV, 2.82 eV and 2.77 eV over 12 h, 24 h and 48 h respectively.[33] In a different investigation, the CeO_2 samples synthesized at different reaction temperature has band gap energies of 2.79 eV, 2.94 eV and 2.77 eV.[50] Therefore, the decrease in the band gap values indicates more oxygen vacancies in the CeO_2 samples, which is in agreement with the Raman spectral analysis.

3.4. Fourier-transform infrared spectroscopy

The FTIR spectra of the CeO_2 NPs at different reaction times are shown in Fig. 5. For the CeO_2 NPs, bands were observed in the region 4000 cm^{-1} 400 cm^{-1}. The broad absorption frequency band at 3000 - 3700 cm^{-1} is allocated to the O-H stretching vibration region of water.[51] The notable peaks, which measured approximately 1300 cm^{-1} and 1650 cm^{-1}, were associated with the O-H vibration mode.[12,52] Some trapped CO_2 in the air could cause the absorption peak in the sample (b) at 2334 cm^{-1}.[53] Ramachandran *et al.* observed that the vibrational peak at 2348 cm^{-1} correlates to the stretching vibration of the C=O bond in CeO. In sample (c), a small peak was identified at 844.7 cm^{-1}, corresponding to the Ce-O stretching vibration.[8] The wavenumber range from 400 cm^{-1} to 500 cm^{-1} is associated with the Ce-O stretching vibration.[54,55] The wavenumbers 405 cm^{-1}, 412 cm^{-1}, 419 cm^{-1}, and 844.7 cm^{-1} confirmed the Ce-O stretching vibration.

3.5 Morphological studies and Elemental analysis

The surface morphologies shown in Fig. 6 (a-c) of the CeO_2 nanoparticles were examined using FESEM. In one study, the morphology was observed to be nearly spherical for samples (a) 12 h and (b) 24 h and cubical for sample (c) 48 h. The particle sizes of the three samples were estimated to be 22, 23, and 70 nm using the ImageJ software. Furthermore, it was observed that the morphology of the product was spherical, comprising agglomerated NPs, which was attributed to a decrease in particle size.[9] According to Abid *et al.*, the surface area is the largest for the smallest particle size and also achieves a spherical morphology by laser ablation in the liquid method.[12] In another study, Ramachandran *et al.* obtained a particle size of 27 nm at pH-12 and a spherical morphology via a modified co-precipitation method.[8] In a different investigation, Li *et al.* obtained shuttle-like CeO_2 NPs using a hydrothermal technique with varying reaction times.[33] In addition to adjusting the reaction temperature, Sehar *et al.* achieved spherical and cubical morphologies using the hydrothermal method.[10]

As seen in Fig. 7, the samples cerium and oxygen contents were examined using EDX. The presence of elemental cerium was 16.14 %, 14.50 %, and 16.92 % for samples (a) 12 h, (b) 24 h, and (c) 48 h, respectively. Likewise, 83.86 %, 85.50 %, and 83.08 % for samples (a) 12 h, (b) 24 h, and (c) 48 h, respectively, confirmed the presence of oxygen. There were no impurities in the EDX spectrum, and this shows that the pure CeO_2 NPs make up the entire final product.

3.6. Antibacterial activity

NPs have been extensively studied to explore their utility as antibacterial agents. NPs are used in biological applications for various reasons, including their low toxicity and resistance. Using ten different concentrations of samples, antibacterial activity against Gram-positive bacteria and Gram-negative bacteria was investigated. The antibacterial activity of CeO_2 NPs was demonstrated using the disc diffusion method. Table 2 and Fig. 8 depict the size of the zone of inhibition and the activity created around each loaded CeO_2 NPs sample. Sample (a) NPs generated an inhibition zone against *E.coli* of 33 mm at 1000 µg/mL and 18 mm at 500 µg/mL. Moreover, sample (b) exhibited an inhibition zone of 16 mm at 1000 µg/ml against *E. coli*, and it showed inhibition zones of 21 mm at 1000 µg/mL and 12 mm at 500 µg/mL against *S. aureus*. No antibacterial activity was observed against both bacteria in sample (c). In addition, the diameter of inhibition increased as the concentration of CeO_2 NPs was raised.[56] Fig. 9 demonstrates the resazurin assay of the samples and positive control ampicillin. The antimicrobial properties of the prepared CeO_2 NPs are compared with results from previous work, as shown in Table 3.

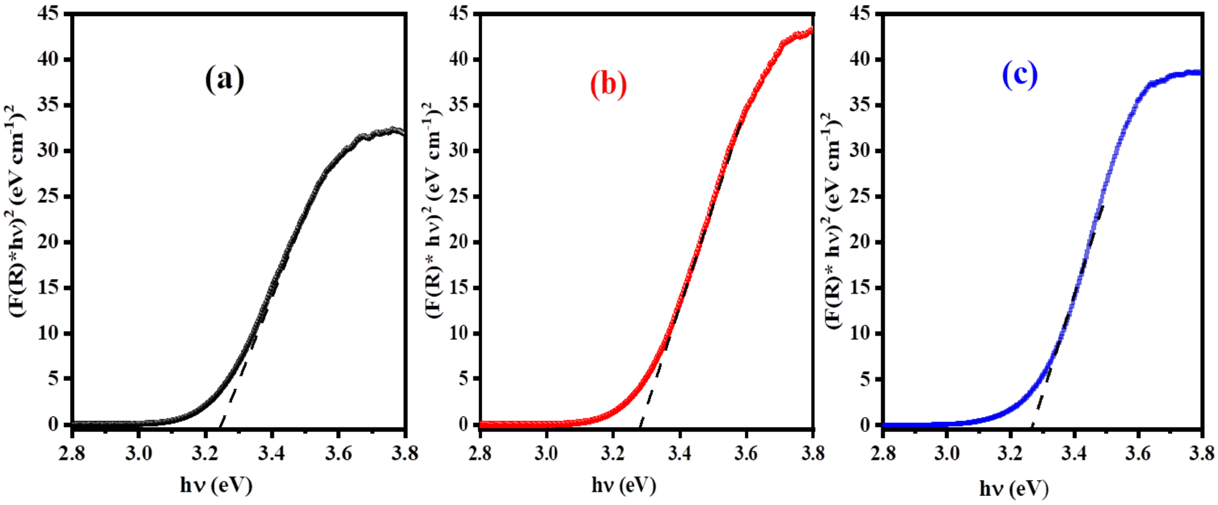

Fig. 4 UV-Vis spectroscopy of CeO_2 NPs for (a) 12 h, (b) 24 h and (c) 48 h.

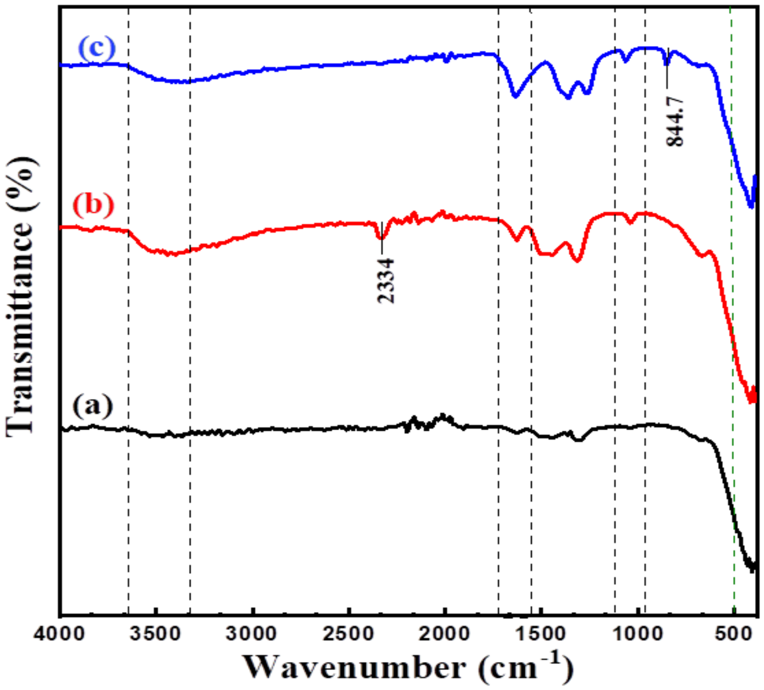

Fig. 5 FTIR spectra of CeO_2 NPs for (a) 12 h, (b) 24 h and (c) 48 h.

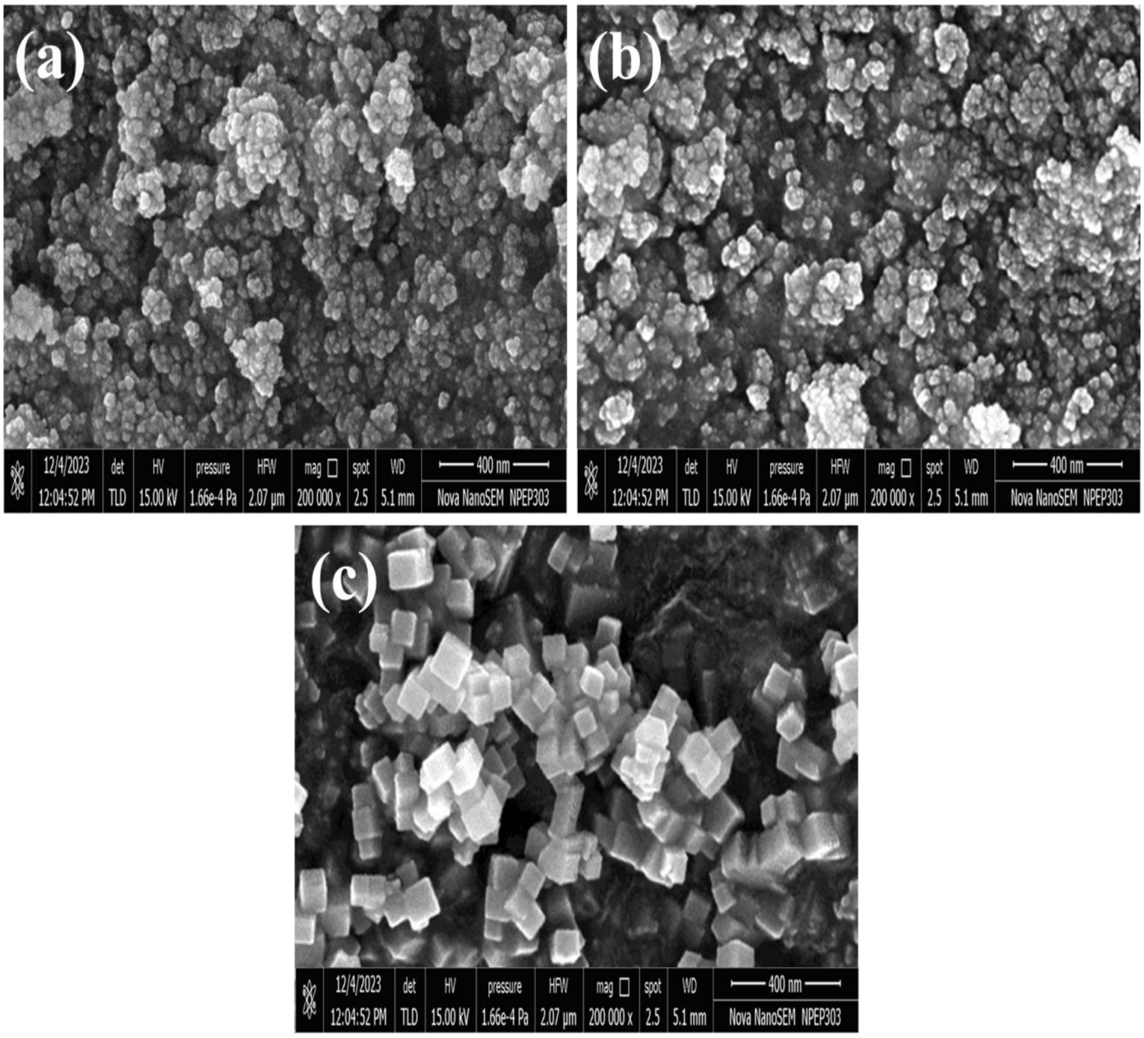

Fig. 6 FESEM images of CeO_2 NPs for (a) 12 h, (b) 24 h and (c) 48 h.

Table 2. Diameter (mm) of the zone of inhibition of Gram-positive and Gram-negative bacteria for samples (a), (b) and (c) with positive control (Ampicillin).

CeO_2 Sample	12 h		24 h		48 h		Ampicillin
	1000 µg/ml	500 µg/ml	1000µg/ml	500µg/ml	1000µg/ml	500 µg/ml	Positive control
E.coli	33 mm	18 mm	16 mm	-	-	-	40 mm
S.aureus	-	-	21 mm	12 mm	-	-	36 mm

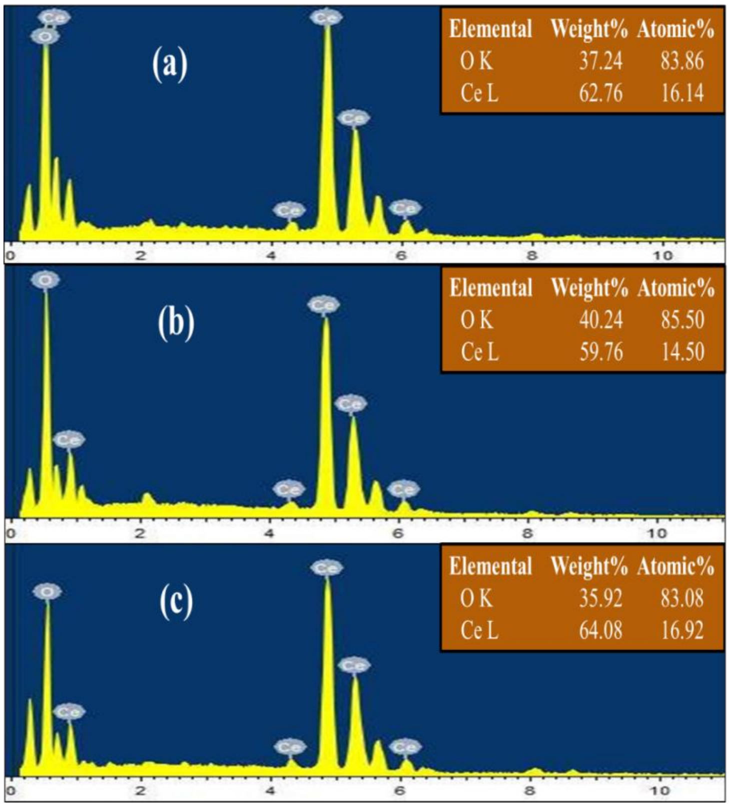

(a)

Elemental	Weight%	Atomic%
O K	37.24	83.86
Ce L	62.76	16.14

(b)

Elemental	Weight%	Atomic%
O K	40.24	85.50
Ce L	59.76	14.50

(c)

Elemental	Weight%	Atomic%
O K	35.92	83.08
Ce L	64.08	16.92

Fig. 7 EDX analysis of CeO_2 NPs (a) 12 h, (b) 24 h, and (c) 48 h.

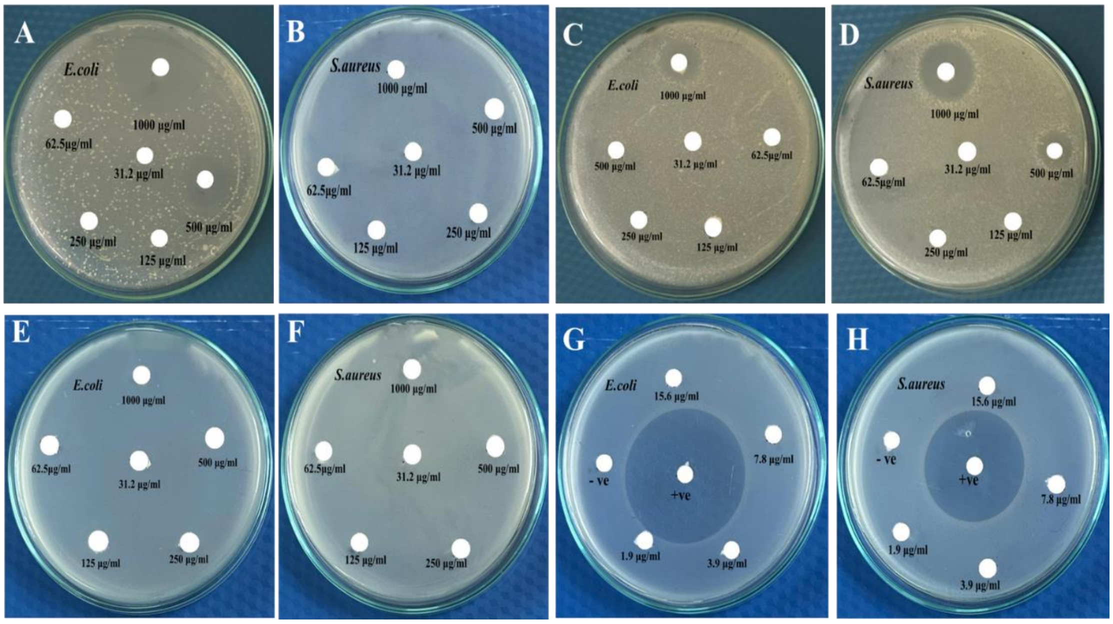

Fig. 8 Inhibition zone of CeO_2 NPs (a) 12 h against E.coli, (b) 24 h against *E.coli and S.aureus*, and (c) 48 h against *E.coli and S.aureus*.

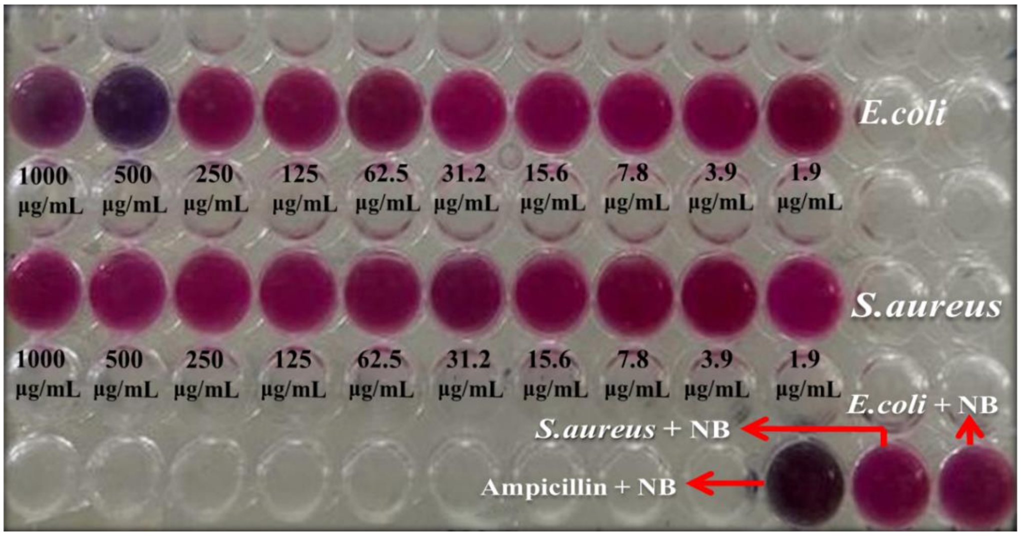

Fig. 9 Minimum inhibitory concentration determination assay using resazurin in microtiter plates. Gram negative bacteria (*E.coli)*, Gram-positive bacteria (*S.aureus*) and, Ampicillin were used as positive control.

Table 3. Compare the current antimicrobial properties results of the prepared CeO_2 NPs with previous work.

Synthesis method of CeO_2 NPs	Morphology	Particle size (nm)	Type of Bacteria/Fungi	Concentration	References
Green synthesis method	spherical	17 nm	*E.coli, S.aureus, P.aeruginosa, C.albicians, A.fumigutas*	100 mg/ml	[21]
Green-hydrothermal approach	spherical	5 to 10 nm	*E.coli* *S.aureus*	40 µg/ml	[22]
Hydrothermal method	spherical and cubical	-	*E.coli* *P.aeruginosa* *B.subtils* *S.aureus*	250 µg/ml 500 µg/ml	[10]
Hydrothermal method	spherical and cubical	22 nm, 23 nm, and 70 nm	*E.coli* *S.aureus*	1000 µg/ml 500 µg/ml	Present work

The effectiveness of CeO_2 NPs against bacteria typically depends on factors such as their specific surface area, electrostatic properties, morphology, and size.[40,56] Generally, the cell walls of Gram-negative bacteria are made up of several layers of lipopolysaccharide, peptidoglycan, and lipid. In contrast, the cell walls of Gram-positive bacteria consist of densely packed peptidoglycan structures. The reason for the significant resistance of Gram-positive bacteria to NPs penetration is their thick layer of peptidoglycan, which is composed of short peptides and linear chains of polysaccharides. Electrostatic interactions between positively charged NPs and negatively charged bacterial cell walls are possible, and NPs can penetrate the cell wall. This interaction has the potential to induce antibacterial activity.[10] Fig. 10 illustrates the antibacterial mechanism of CeO_2 NPs. The antimicrobial impact of CeO_2 NPs is elucidated by the electrostatics between CeO_2 NPs and microorganisms. It leads to cellular modification and generation of ROS, ultimately resulting in biological activity.[57,58] The generation of reactive oxygen species (ROS) by CeO_2 NPs damages the lipids in cell membranes, resulting in a loss of membrane integrity. They also cause DNA strand breakage as well as alter and deactivate vital proteins. Moreover, biomolecules in the bacterial cell membrane are attached by Ce^{3+} ions through electrostatic interactions, which results in cellular leakage and death. Fig. 11 shows the percentage inhibition and concentration effect of samples on *E. coli, S. aureus,* ampicillin (positive control), and Double distilled water (DDW) used as negative control.

The MIC is the smallest amount of an antimicrobial agent, such as an antibiotic, that hinders the growth of a specific microorganism. This serves as a quantitative gauge of the efficacy of an antimicrobial agent against a particular bacterial strain. The 96-well plate method, based on resazurin, is a straightforward and highly accurate approach for determining MIC. Resazurin, a blue dye, transforms into resorufin (pink) in the presence of active bacterial cells. The MIC is typically identified by testing antimicrobial agents against microorganisms in a series of dilutions, often in a liquid grow-

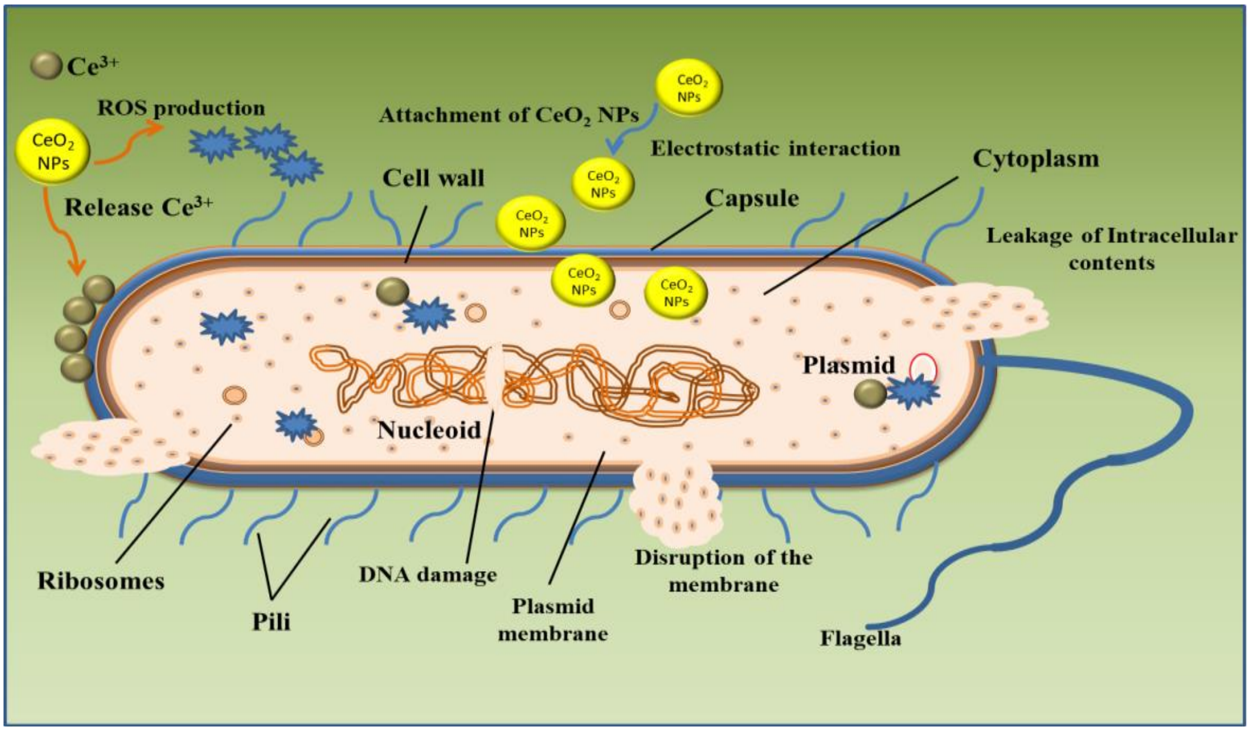

Fig. 10 Antibacterial mechanism of cerium oxide nanoparticles.

-th medium. The MIC is the concentration at which the blue color persists. Moreover, no Minimum Bactericidal Concentration (MBC) was observed against both bacteria. Fig. 12 shows the MBC obtained using the drop-plate technique. The reaction times are the key parameters for controlling the morphology and particle size. According to FESEM analysis Fig. 6, spherical CeO_2 NPs showed the smallest particle size. These findings show that all CeO_2 NPs have antibacterial properties against both Gram-positive bacteria and Gram-negative bacteria. Hence, the spherical morphology exhibited better antibacterial activity than the cubical morphology. Abid *et al.* achieved a spherical morphology with particle sizes ranging from 26 to 37 nm and investigated their antibacterial activity against *P. aeruginosa, E. coli,* and *S.aureus.*[12]

3.7 Bacterial cell morphology

Figures 13 and 14 show the effects of cerium oxide nanoparticles on the morphology of two bacterial strains. When the bacterial strains *S. aureus* and *E. coli* were not treated with nanoparticles, their cells seemed smooth and unharmed. Nevertheless, there were noticeable morphological alterations in the two bacterial strains when they were exposed

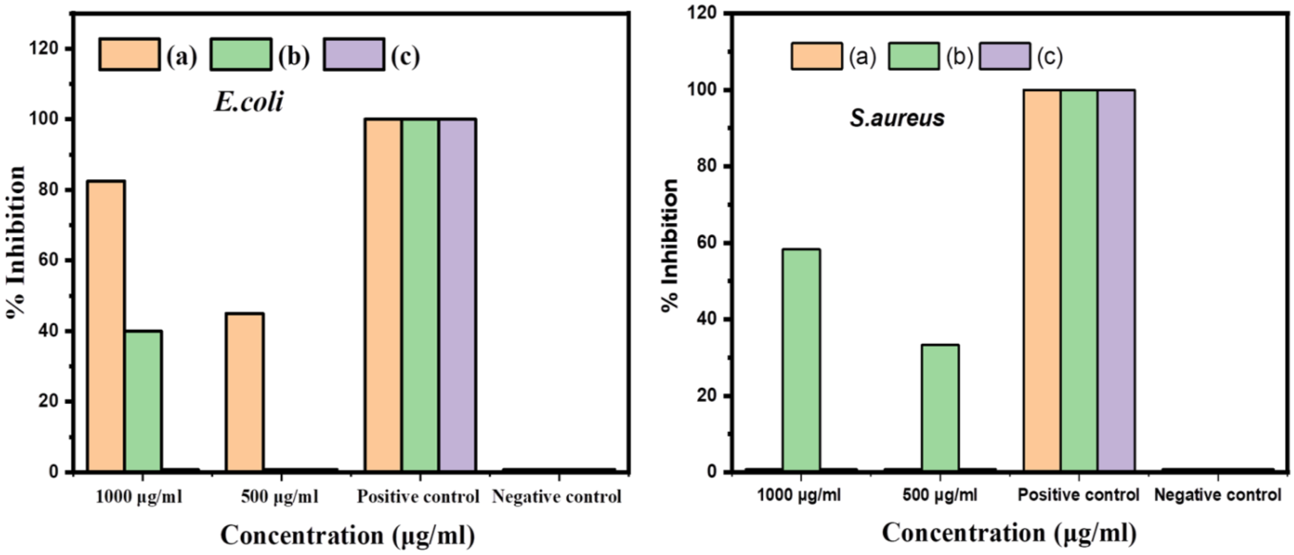

Fig. 11 The percentage inhibition zone concentration effect of samples on *E.coli* and *S.aureus* of samples (a) 12 h, (b) 24 h and (c) 48 h, Ampicillin (positive control) and DDW (Negative control).

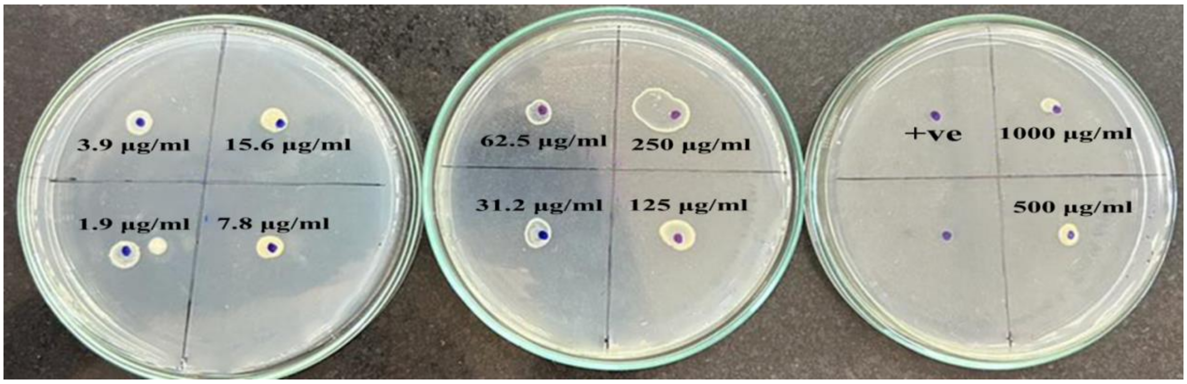

Fig. 12 Minimum Bactericidal Concentration using the drop plate technique.

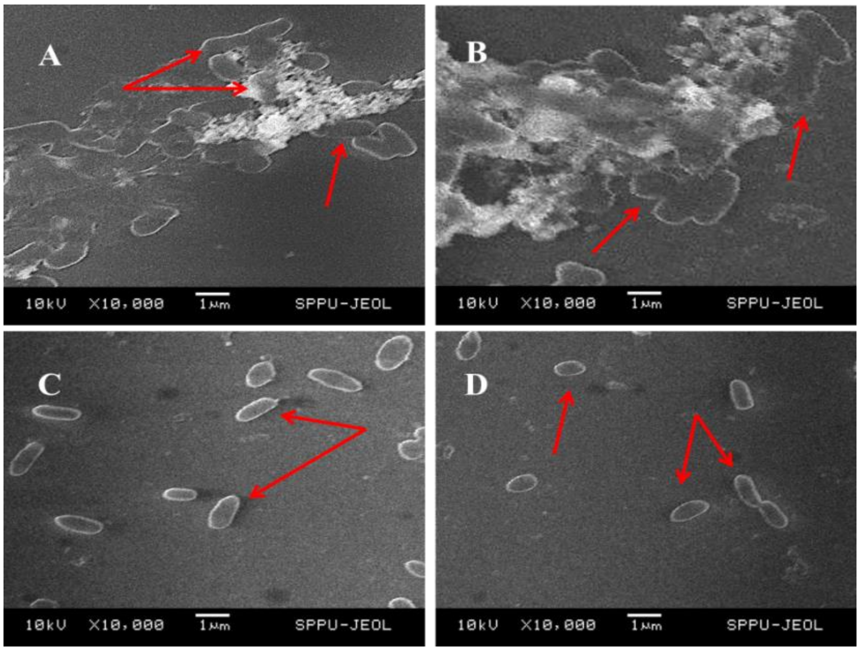

Fig. 13 Effect of CeO_2 NPs synthesis conditions on *E.coli* bacteria cell morphology by scanning electron microscope (A) 12 h, (B) 24 h and (C) 48 h respectively and (D) control (normal cells).

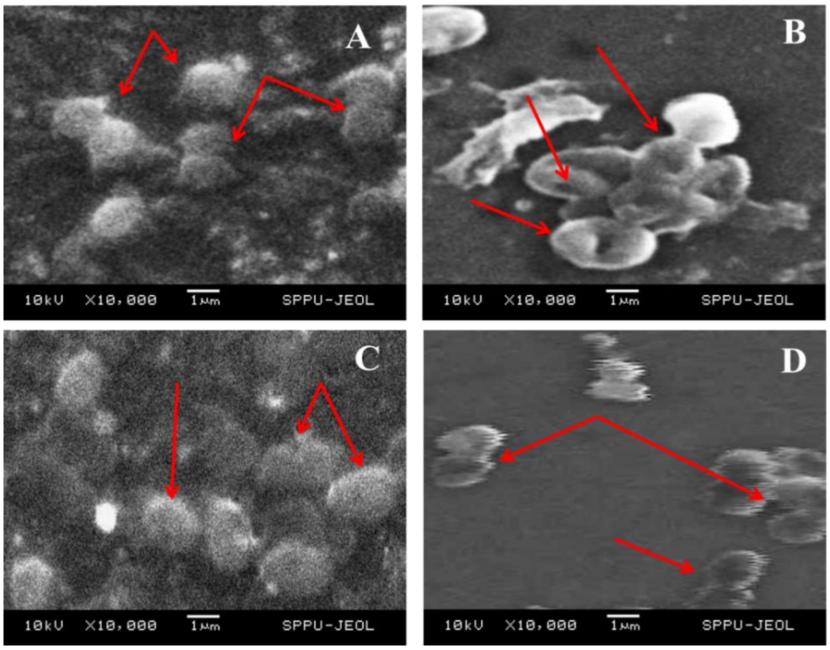

Fig. 14 Effect of CeO_2 NPs synthesis conditions on *S.aureus* bacteria cell morphology by scanning electron microscope (A) 12 h, (B) 24 h and (C) 48 h respectively and (D) control (normal cells).

to NPs. Following incubation, the bacteria displayed rumples and lost their morphological shape as a result of the CeO_2 NPs damaging the integrity of the bacterial cell membranes. This suggests that the morphology of bacterial cells is negatively impacted by CeO_2 NPs, which results in considerable damage to the cell wall.[59]

4. Conclusion

Hydrothermal method was employed successfully for the synthesize of CeO_2 nanoparticles at different reaction times. The findings confirmed that the reaction time affects the structural and optical properties of CeO_2 NPs. The average crystallite size ranged from 9 nm to 19 nm, indicating a significant variation in the crystal size. Raman spectra revealed a band around 463 cm^{-1}, corresponding to the F2g optical phonon mode linked to the stretching Ce-O vibration. Using diffuse reflectance spectroscopy, the optical energy bandgap of the CeO_2 NPs was found to be 3.2 to 3.3 eV. FTIR confirmed the Ce-O stretching vibrations. FESEM analysis indicated spherical and cubical morphologies with an average diameter of 24 nm and 70 nm respectively. Due to the presence of high intensity peaks in the EDX analysis, the samples were found to contain pure oxygen and cerium. The results demonstrated that smaller particles and higher surface areas exhibited enhanced antibacterial activity. Understanding the correlation between nanoparticles morphology and antibacterial activity is pivotal for developing effective antibacterial agents. Additionally, this study revealed that the spherical morphology exhibited superior antibacterial performance against both bacteria compared with the cubical morphology. Consequently, the study concludes that the synthesized CeO_2 NPs are promising candidates for biomedical applications.

Conflict of Interest

There is no conflict of interest.

Supporting Information

Not applicable.

References

[1] A. Gupta, S. Mumtaz, C.-H. Li, I. Hussain, V. M. Rotello, Combatting antibiotic-resistant bacteria using nanomaterials, *Chemical Society Reviews*, 2019, **48**, 415-427, doi: 10.1039/c7cs00748e.

[2] F. Charbgoo, M. Ramezani, M. Darroudi, Bio-sensing applications of cerium oxide nanoparticles: advantages and disadvantages, *Biosensors and Bioelectronics*, 2017, **96**, 33-43, doi: 10.1016/j.bios.2017.04.037.

[3] C. Walkey, S. Das, S. Seal, J. Erlichman, K. Heckman, L. Ghibelli, E. Traversa, J. F. McGinnis, W. T. Self, Catalytic properties and biomedical applications of cerium oxide nanoparticles, *Environmental Science: Nano*, 2015, **2**, 33-53, doi: 10.1039/c4en00138a.

[4] N. Afza, M. S. Shivakumar, M. W. Alam, A. N. Kumar, A. S. Bhatt, H. C. A. Murthy, C. R. Ravikumar, M. Mylarappa, S. Selvanandan, Facile hydrothermal synthesis of cerium oxide/rGO nanocomposite for photocatalytic and supercapacitor applications, *Applied Surface Science Advances*, 2022, **11**, 100307, doi: 10.1016/j.apsadv.2022.100307.

[5] O. L. Pop, A. Mesaros, D. C. Vodnar, R. Suharoschi, F. Tăbăran, L. Mageruşan, I. S. Tódor, Z. Diaconeasa, A. Balint, L. Ciontea, C. Socaciu, Cerium oxide nanoparticles and their efficient antibacterial application *in vitro* against gram-positive and gram-negative pathogens, *Nanomaterials*, 2020, **10**, 1614, doi: 10.3390/nano10081614.

[6] M. Pešić, A. Podolski-Renić, S. Stojković, B. Matović, D. Zmejkoski, V. Kojić, G. Bogdanović, A. Pavićević, M. Mojović, A. Savić, I. Milenković, A. Kalauzi, K. Radotić, Anti-cancer effects of cerium oxide nanoparticles and its intracellular redox activity, *Chemico-Biological Interactions*, 2015, **232**, 85-93, doi: 10.1016/j.cbi.2015.03.013.

[7] Y. Shlapa, S. Solopan, V. Sarnatskaya, K. Siposova, I. Garcarova, K. Veltruska, I. Timashkov, O. Lykhova, D. Kolesnik, A. Musatov, V. Nikolaev, A. Belous, Cerium dioxide nanoparticles synthesized via precipitation at constant pH: synthesis, physical-chemical and antioxidant properties, *Colloids and Surfaces B: Biointerfaces*, 2022, **220**, 112960, doi: 10.1016/j.colsurfb.2022.112960.

[8] M. Ramachandran, R. Subadevi, M. Sivakumar, Role of pH on synthesis and characterization of cerium oxide (CeO_2) nano particles by modified co-precipitation method, *Vacuum*, 2019, **161**, 220-224, doi: 10.1016/j.vacuum.2018.12.002.

[9] M. Panahi-Kalamuei, S. Alizadeh, M. Mousavi-Kamazani, M. Salavati-Niasari, Synthesis and characterization of CeO_2 nanoparticles via hydrothermal route, *Journal of Industrial and Engineering Chemistry*, 2015, **21**, 1301-1305, doi: 10.1016/j.jiec.2014.05.046.

[10] S. Sehar, I. Naz, A. Rehman, W. Sun, S. S. Alhewairini, M. N. Zahid, A. Younis, Shape-controlled synthesis of cerium oxide nanoparticles for efficient dye photodegradation and antibacterial activities, *Applied Organometallic Chemistry*, 2021, **35**, e6069, doi: 10.1002/aoc.6069.

[11] E. Kumar, P. Selvarajan, D. Muthuraj, Synthesis and characterization of CeO_2 nanocrystals by solvothermal route, *Materials Research*, 2013, **16**, 269-276, doi: 10.1590/s1516-14392013005000021.

[12] S. A. Abid, A. A. Taha, R. A. Ismail, M. H. Mohsin, Antibacterial and cytotoxic activities of cerium oxide nanoparticles prepared by laser ablation in liquid, *Environmental Science and Pollution Research*, 2020, **27**, 30479-30489, doi: 10.1007/s11356-020-09332-9.

[13] S. Kontham, K. Mandava, S. Dosa, F. U. Mohd, O. A. Mohammed, A. U. Mohammad, Review on facile synthesis of cerium oxide nanoparticles and their biomedical applications, *Inorganic and Nano-Metal Chemistry*, 2022, **52**, 1183-1195, doi: 10.1080/24701556.2021.1963284.

[14] M. Zarezadeh Mehrizi, S. Ahmadi, R. Beygi, M. Asadi, Fabrication of cerium oxide nanoparticles by solution combustion

synthesis and their cytotoxicity evaluation, *Russian Journal of Non-Ferrous Metals*, 2018, **59**, 111-116, doi: 10.3103/s1067821218010170.

[15] A. S. Fudala, W. M. Salih, F. F. Alkazaz, Synthesis different sizes of cerium oxide CeO_2 nanoparticles by using different concentrations of precursor via sol–gel method, *Materials Today: Proceedings*, 2022, **49**, 2786-2792, doi: 10.1016/j.matpr.2021.09.452.

[16] J. Xu, C. Zhang, Oxygen vacancy engineering on cerium oxide nanowires for room-temperature linalool detection in rice aging, *Journal of Advanced Ceramics*, 2022, **11**, 1559-1570, doi: 10.1007/s40145-022-0629-8.

[17] M. Khairy, A synergetic effect of cerium oxide nanocubes and gold nanoparticles for developing a new photoelectrochemical sensor of codeine drug, *Journal of Electroanalytical Chemistry*, 2021, **895**, 115517, doi: 10.1016/j.jelechem.2021.115517.

[18] C. Brambila, J. Nutter, M. Molinari, D. C. Sayle, T. Sakthivel, S. Seal, G. Möbus, Void space and secondary oriented attachment mechanisms in cerium oxide nanorods, *Journal of Nanoparticle Research*, 2022, **24**, 227, doi: 10.1007/s11051-022-05598-x.

[19] M. Zhang, C. Zhang, X. Zhai, F. Luo, Y. Du, C. Yan, Antibacterial mechanism and activity of cerium oxide nanoparticles, *Science China Materials*, 2019, **62**, 1727-1739, doi: 10.1007/s40843-019-9471-7.

[20] K. M. Kumar, M. Mahendhiran, M. C. Diaz, N. Hernandez-Como, A. Hernandez-Eligio, G. Torres-Torres, S. Godavarthi, L. M. Gomez, Green synthesis of Ce_3 + rich CeO_2 nanoparticles and its antimicrobial studies, *Materials Letters*, 2018, **214**, 15-19, doi: 10.1016/j.matlet.2017.11.097.

[21] G. Eka Putri, Y. Rilda, S. Syukri, A. Labanni, S. Arief, Highly antimicrobial activity of cerium oxide nanoparticles synthesized using Moringa oleifera leaf extract by a rapid green precipitation method, *Journal of Materials Research and Technology*, 2021, **15**, 2355-2364, doi: 10.1016/j.jmrt.2021.09.075.

[22] H. Siddiqui, S. Kumar, P. Naidu, S. Gupta, S. Mishra, M. Goswami, P. K. Sairkar, L. Atram, N. Sathish, S. Kumar, Solanum tuberosum tuber-driven starch-mediated green-hydrothermal synthesis of cerium oxide nanoparticles for efficient photocatalysis and antimicrobial activities, *Chemosphere*, 2024, **352**, 141418, doi: 10.1016/j.chemosphere.2024.141418.

[23] L. Wang, C. Hu, L. Shao, The antimicrobial activity of nanoparticles: present situation and prospects for the future, *International Journal of Nanomedicine*, 2017, **12**, 1227-1249, doi: 10.2147/ijn.s121956.

[24] M. Nadeem, R. Khan, K. Afridi, A. Nadhman, S. Ullah, S. Faisal, Z. U. Mabood, C. Hano, B. H. Abbasi, Green synthesis of cerium oxide nanoparticles (CeO_2 NPs) and their antimicrobial applications: a review, *International Journal of Nanomedicine*, 2020, **15**, 5951-5961, doi: 10.2147/ijn.s255784.

[25] S. Pansambal, R. Oza, S. Borgave, A. Chauhan, P. Bardapurkar, S. Vyas, S. Ghotekar, Bioengineered cerium oxide (CeO_2) nanoparticles and their diverse applications: a review, *Applied Nanoscience*, 2023, **13**, 6067-6092, doi: 10.1007/s13204-022-02574-8.

[26] M. Alekish, Z. B. Ismail, B. Albiss, S. Nawasrah, *In vitro* antibacterial effects of zinc oxide nanoparticles on multiple drug-resistant strains of Staphylococcus aureus and Escherichia coli: an alternative approach for antibacterial therapy of mastitis in sheep, *Veterinary World*, 2018, **11**, 1428-1432, doi: 10.14202/vetworld.2018.1428-1432.

[27] S. Chen, Z. Li, Z. Gu, X. Ban, Y. Hong, L. Cheng, C. Li, A new micro-agar dilution method to determine the minimum inhibitory concentration of essential oils against microorganisms, *Journal of Microbiological Methods*, 2023, **211**, 106791, doi: 10.1016/j.mimet.2023.106791.

[28] S. D. Sarker, L. Nahar, Y. Kumarasamy, Microtitre plate-based antibacterial assay incorporating resazurin as an indicator of cell growth, and its application in the *in vitro* antibacterial screening of phytochemicals, *Methods*, 2007, **42**, 321-324, doi: 10.1016/j.ymeth.2007.01.006.

[29] M. Elshikh, S. Ahmed, S. Funston, P. Dunlop, M. McGaw, R. Marchant, I. M. Banat, Resazurin-based 96-well plate microdilution method for the determination of minimum inhibitory concentration of biosurfactants, *Biotechnology Letters*, 2016, **38**, 1015-1019, doi: 10.1007/s10529-016-2079-2.

[30] C. Chakansin, J. Yostaworakul, C. Warin, K. Kulthong, S. Boonrungsiman, Resazurin rapid screening for antibacterial activities of organic and inorganic nanoparticles: potential, limitations and precautions, *Analytical Biochemistry*, 2022, **637**, 114449, doi: 10.1016/j.ab.2021.114449.

[31] Y. Asahi, J. Miura, T. Tsuda, S. Kuwabata, K. Tsunashima, Y. Noiri, T. Sakata, S. Ebisu, M. Hayashi, Simple observation of Streptococcus mutans biofilm by scanning electron microscopy using ionic liquids, *AMB Express*, 2015, **5**, 1-9, doi: 10.1186/s13568-015-0097-4.

[32] V. Pathak, P. Lad, A. B. Thakkar, P. Thakor, M. P. Deshpande, S. Pandya, Synthesis, characterization and applications of cubic fluorite cerium oxide nanoparticles: a comprehensive study, *Results in Surfaces and Interfaces*, 2023, **11**, 100111, doi: 10.1016/j.rsurfi.2023.100111.

[33] H. Li, F. Meng, J. Gong, Z. Fan, R. Qin, Structural, morphological and optical properties of shuttle-like CeO_2 synthesized by a facile hydrothermal method, *Journal of Alloys and Compounds*, 2017, **722**, 489-498, doi: 10.1016/j.jallcom.2017.06.156.

[34] F. Ozel, H. Kockar, O. Karaagac, Growth of iron oxide nanoparticles by hydrothermal process: effect of reaction parameters on the nanoparticle size, *Journal of Superconductivity and Novel Magnetism*, 2015, **28**, 823-829, doi: 10.1007/s10948-014-2707-9.

[35] A. I. Y. Tok, F. Y. C. Boey, Z. Dong, X. L. Sun, Hydrothermal synthesis of CeO_2 nano-particles, *Journal of Materials Processing Technology*, 2007, **190**, 217-222, doi: 10.1016/j.jmatprotec.2007.02.042.

[36] B. D. Cullity, Elements of X-ray Diffraction. United Kingdom: Addison-Wesley Publishing Company,1956.

[37] A. Ukarande, M. V. Salve, S. Chaure, O. I. Olusola, T. M. W. J. Bandara, M. Furlani, B.-E. Mellander, M. A. K. L. Dissanayake, I. Albinsson, N. B. Chaure, Investigation of electrodeposited CdTe thin films for solar cell development, *Journal of Materials Science: Materials in Electronics*, 2023, **34**, 1887, doi: 10.1007/s10854-023-11337-2.

[38] X. Venci, A. George, S. Rahul, A. Dhayal Raj, A. Albert Irudayaraj, R. L. Josephine, S. John Sundaram, K. Kaviyarasu, Investigation on the formation of self-assembled CdSe dendrite structures and their photocatalytic efficiency, *Inorganic Chemistry Communications*, 2023, **148**, 110309, doi: 10.1016/j.inoche.2022.110309.

[39] Y. B. Chan, M. Aminuzzaman, L.-H. Tey, Y. F. Win, A. Watanabe, S. Djearamame, M. Akhtaruzzaman, Impact of diverse parameters on the physicochemical characteristics of green-synthesized zinc oxide–copper oxide nanocomposites derived from an aqueous extract of garcinia mangostana L. leaf, *Materials*, 2023, **16**, 5421, doi: 10.3390/ma16155421.

[40] Y. B. Chan, M. Aminuzzaman, M. K. Rahman, Y. F. Win, S. Sultana, S.-Y. Cheah, A. Watanabe, L. S. Wong, S. K. Guha, S. Djearamane, V. Rajendran, M. Akhtaruzzaman, L.-H. Tey, Green synthesis of ZnO nanoparticles using the mangosteen (*Garcinia mangostana* L.) leaf extract: comparative preliminary *in vitro* antibacterial study, *Green Processing and Synthesis*, 2024, **13**, 20230251, doi: 10.1515/gps-2023-0251.

[41] G. Jayakumar, A. Albert Irudayaraj, A. Dhayal Raj, A comprehensive investigation on the properties of nanostructured cerium oxide, *Optical and Quantum Electronics*, 2019, **51**, 312, doi: 10.1007/s11082-019-2029-z.

[42] E. K. Goharshadi, S. Samiee, P. Nancarrow, Fabrication of cerium oxide nanoparticles: characterization and optical properties, *Journal of Colloid and Interface Science*, 2011, **356**, 473-480, doi: 10.1016/j.jcis.2011.01.063.

[43] A. R. Rajan, V. Vilas, A. Rajan, A. John, D. Philip, Synthesis of nanostructured CeO_2 by chemical and biogenic methods: optical properties and bioactivity, *Ceramics International*, 2020, **46**, 14048-14055, doi: 10.1016/j.ceramint.2020.02.204.

[44] N. Pandiyan, B. Murugesan, J. Sonamuthu, S. Samayanan, S. Mahalingam, Facile biological synthetic strategy to morphologically aligned CeO_2/ZrO_2 core nanoparticles using Justicia adhatoda extract and ionic liquid: enhancement of its bio-medical properties, *Journal of Photochemistry and Photobiology B: Biology*, 2018, **178**, 481-488, doi: 10.1016/j.jphotobiol.2017.11.036.

[45] K. Govindarasu, K. Gnanasekaran, S. Balaraman, B. Iruson, S. Krishnamoorthy, S. Balaraman, B. Padmaraj, E. Manikandan, S. Dhananjayan, Study on enhanced antibacterial and cytotoxicity of pure and cadmium doped cerium oxide against gram-positive and gram-negative bacteria, *Soft Nanoscience Letters*, 2019, **9**, 1-16, doi: 10.4236/snl.2019.91001.

[46] A. Martínez-Arias, M. Fernández-García, L. N. Salamanca, R. X. Valenzuela, J. C. Conesa, J. Soria, Structural and redox properties of ceria in alumina-supported ceria catalyst supports, *The Journal of Physical Chemistry B*, 2000, **104**, 4038-4046, doi: 10.1021/jp992796y.

[47] M. A. Majeed Khan, W. Khan, M. Ahamed, A. N. Alhazaa, Microstructural properties and enhanced photocatalytic performance of Zn doped CeO_2 nanocrystals, *Scientific Reports*, 2017, **7**, 12560, doi: 10.1038/s41598-017-11074-7.

[48] A. Martinezarias, D. Gamarra, M. Fernandezgarcia, X. Wang, J. Hanson, J. Rodriguez, Comparative study on redox properties of nanosized CeO_2 and CuO/CeO_2 under CO/O2, *Journal of Catalysis*, 2006, **240**, 1-7, doi: 10.1016/j.jcat.2006.02.026.

[49] R.W. Frei, Diffuse Reflectance Spectroscopy Environmental Problem Solving, United States: CRC Press, 2019.

[50] L. Qin, X. Niu, Controlled hydrothermal synthesis, excellent optical and magnetic properties of CeO_2 nanocubes, *Journal of Materials Science: Materials in Electronics*, 2016, **27**, 12233-12239, doi: 10.1007/s10854-016-5379-3.

[51] S. Parvathy, G. Manjula, R. Balachandar, R. Subbaiya, Green synthesis and characterization of cerium oxide nanoparticles from Artabotrys hexapetalus leaf extract and its antibacterial and anticancer properties, *Materials Letters*, 2022, **314**, 131811, doi: 10.1016/j.matlet.2022.131811.

[52] R. Zamiri, H. Abbastabar Ahangar, A. Kaushal, A. Zakaria, G. Zamiri, D. Tobaldi, J. M. F. Ferreira, Dielectrical properties of CeO_2 nanoparticles at different temperatures, *PLoS One*, 2015, **10**, e0122989, doi: 10.1371/journal.pone.0122989.

[53] K. Sakthiraj, B. Karthikeyan, Synthesis and characterization of cerium oxide nanoparticles using different solvents for electrochemical applications, *Applied Physics A*, 2019, **126**, 52, doi: 10.1007/s00339-019-3227-z.

[54] B. S. Wee, S. A. bin Eddie Halim, T. F. Choo, Simple hydrothermal synthesis of ultra-small cerium oxide nanoparticles, *Journal of Cluster Science*, 2024, **35**, 2061-2068, doi: 10.1007/s10876-024-02644-7.

[55] I.-T. Liu, M.-H. Hon, L. G. Teoh, Structure and optical properties of CeO_2 nanoparticles synthesized by precipitation, *Journal of Electronic Materials*, 2013, **42**, 2536-2541, doi: 10.1007/s11664-013-2617-9.

[56] V. Selvanathan, M. Aminuzzaman, L. X. Tan, Y. F. Win, E. S. Guan Cheah, M. H. Heng, L.-H. Tey, S. Arullappan, N. Algethami, S. S. Alharthi, S. Sultana, M. Shahiduzzaman, H. Abdullah, M. Aktharuzzaman, Synthesis, characterization, and preliminary invitro antibacterial evaluation of ZnO nanoparticles derived from soursop (Annona muricata L.) leaf extract as a green reducing agent, *Journal of Materials Research and Technology*, 2022, **20**, 2931-2941, doi: 10.1016/j.jmrt.2022.08.028.

[57] H. Qiu, F. Pu, Z. Liu, Q. Deng, P. Sun, J. Ren, X. Qu, Depriving bacterial adhesion-related molecule to inhibit biofilm formation using CeO_2-decorated metal-organic frameworks, *Small*, 2019, **15**, 1902522, doi: 10.1002/smll.201902522.

[58] X. Fan, L. Yahia, E. Sacher, Antimicrobial properties of the Ag, Cu nanoparticle system, *Biology*, 2021, **10**, 137, doi: 10.3390/biology10020137.

[59] F. Y. Rezaei, G. Pircheraghi, V. S. Nikbin, Antibacterial activity, cell wall damage, and cytotoxicity of zinc oxide nanospheres, nanorods, and nanoflowers, *ACS Applied Nano Materials*, 2024, **7**, 15242-15254, doi: 10.1021/acsanm.4c02046.